IEEE Access
Multidisciplinary ⋮ Rapid Review ⋮ Open Access Journal

Received 31 December 2023, accepted 24 January 2024, date of publication 8 February 2024, date of current version 4 April 2024.

Digital Object Identifier 10.1109/ACCESS.2024.3364068

RESEARCH ARTICLE

Combined Localization Method for Multimodal Wheel-Track Robots in Sheltered Space

JIAZHEN LIN, ZHONG SU, (Member, IEEE), HUI ZHAO, YUXIN ZHAO, XINKAI WANG, AND HAO ZHOU

School of Automation, Beijing Information Science and Technology University, Beijing 100192, China
Beijing Key Laboratory of High Dynamic Navigation Technology, Beijing 100192, China

Corresponding author: Zhong Su (sz@bistu.edu.cn)

This work was supported in part by the National Key Research and Development Program of China under Grant 2020YFC1511702 and Grant 2022YFF0607400; in part by the National Natural Science Foundation of China under Grant 61971048; in part by Beijing Science and Technology Project under Grant Z221100005222024; and in part by Beijing Scholars Program, Key Laboratory of Modern Measurement and Control Technology, Ministry of Education.

ABSTRACT In response to the localization challenges posed by multi-modal motion mode transitions during the locomotion of tracked-wheel robots in sheltered spaces, this paper presents a combination localization method based on Inertial Navigation System/Odometry (INS/OD). Leveraging the unique locomotion structure of tracked-wheel robots, a multi-modal odometry motion model and non-holonomic constrained (NHC) velocity model are established. A closed-loop extended Kalman filter is employed to construct the combination localization model, facilitating real-time computation and correction of the robot's heading angle using the odometry motion model, effectively mitigating system errors and preventing heading divergence. The wheeled-track robot was subjected to outdoor and underground tunnel real-world localization tests. The results demonstrate that the proposed combined localization method achieved an absolute positioning accuracy of the wheeled-track robot within 0.3578 meters in outdoor experiments. This accounts for only 0.31% of the total distance traveled in the outdoor experiments, with an average error of 0.1611 meters. In the context of relative positioning within the underground tunnel, the localization error was measured at 0.2143 meters, representing a mere 0.2306% of the total distance covered in the tunnel. These findings affirm the capability of the combined localization method to meet the practical localization requirements of the wheeled-track robot, both in outdoor and in-sheltered space tunnel scenarios.

INDEX TERMS Sheltered spaces, NHC, multi-modal motion, tracked-wheel robots, inertial navigation system/odometry (INS/OD).

I. INTRODUCTION

In the face of major natural disasters, such as earthquakes, which can lead to unstable underground and sheltered structural space with unknown information, it becomes perilous for rescue personnel to venture into these spaces without due precautions. This is where the deployment of mobile robots becomes imperative to perform various search and rescue tasks, information gathering, and other critical missions in place of human personnel. Underground and sheltered space are characterized by a range of distinctive features, including narrowness, restricted space, inherent hazards, and disorder, which demand that mobile robots possess substantial environmental adaptability and maneuverability to cope with various intricate terrains. Researchers have addressed these demands by designing specialized robots with tracked-wheel structures [1], capable of seamless transitions between tracked and wheeled locomotion modes. This adaptability enhances their flexibility in traversing diverse complex terrains, obstacle navigation capabilities, and overall stability [2]. However, achieving accurate localization of these tracked-wheel robots within sheltered spaces serves as a fundamental prerequisite for enabling advanced applications such as autonomous navigation, simultaneous localization and mapping (SLAM), and other high-level tasks in sheltered space.

Due to the unique characteristics of underground and sheltered spaces, characterized by narrowness, confinement,

The associate editor coordinating the review of this manuscript and approving it for publication was Li He.

hazards, and disorder, autonomous robot localization in sheltered spaces has become a challenging and highly-relevant topic in the field of navigation and localization. Hu et al. [3]. developed a dynamic fusion localization framework based on factor graphs, utilizing Ultra Wide Band (UWB) and Inertial Navigation System (INS) technologies to achieve low-cost robot localization in satellite-denied environments. Nevertheless, sheltered spaces are often elongated, enclosed areas, where UWB localization performance is restricted. Furthermore, UWB technology requires the cumbersome deployment of base stations and may prove intricate to implement. Gao et al. [4]. proposed a robust single-camera visual-inertial-depth odometry (VIDO) for satellite-denied environments, facilitating 6-degree-of-freedom pose estimation without relying on prior information. While this approach offers valuable insights for localization in satellite-denied environments, the complex lighting conditions and environmental factors such as fog, smoke, and dust in underground and sheltered spaces make visual odometry [5] less reliable, leading to challenges in ensuring accurate localization. In the context of underground coal mining, Jiangtao [6] et al. introduced a laser-assisted inertial localization method for coal mining machines, effectively addressing the issue of inertial navigation errors leading to a decline in positioning accuracy over time, thus improving the localization precision of mining robots. However, laser sensors come with limitations, including high costs associated with high-resolution requirements, poor real-time performance, and the challenges posed by diverse and complex obstacles in sheltered spaces, which can impact their reflective performance and consequently restrict their utilization in sheltered spaces localization.

Tracked-wheel robots, in order to adapt to the complex ground environments in sheltered spaces, often require seamless transitioning between wheel and track locomotion modes. However, the use of different coordinate systems and reference points in these distinct modes leads to discontinuities in localization information, resulting in accuracy issues during transitions. Furthermore, different locomotion modes typically necessitate different motion models due to the differing motion characteristics between wheel-based and tracked locomotion. During mode transitions, the robot must adapt to these varying motion models, potentially leading to instability in localization. The unique multi-modal switching characteristic of tracked-wheel robots presents a challenge in terms of localization. Inertial Navigation System/Odometry (INS/OD) combinations, on the other hand, frequently generate measurement data for position and attitude at high frequencies, enabling multiple position estimates in very short time intervals. This continuous stream of localization information helps bridge the position gaps during mode transitions, ensuring the continuity of localization is maintained during such transitions, which is crucial for maintaining accuracy. Moreover, INS/OD combinations offer real-time and continuous localization, allowing robots to obtain immediate position information at the moment of mode transitions, providing uninterrupted localization information. This feature helps prevent lag in localization information during transitions, ultimately reducing localization errors. INS, based on inertial principles, can continuously measure the carrier's position, velocity, attitude, and other information without the need for external interaction, making it suitable for post-disaster complex and adverse environments. However, it suffers from significant error divergence over time. Odometry measures the carrier's distance information but cannot provide absolute position information. INS/OD combination localization can effectively complement each other, enhancing navigation accuracy [7]. This combination method demonstrates high autonomy [8] and interference resistance relative to other mentioned localization methods, making it exceptionally adaptable to sheltered spaces [9], [10], [11] Traditional INS/OD combination localization solutions are usually tailored to single-mode applications, either wheel-based or tracked locomotion, without considering the discontinuity issue associated with multi-mode locomotion transitions.

To address the aforementioned challenges, this paper proposes a multi-modal localization method for tracked-wheel robots based on the INS/OD combination. Leveraging the multi-modal motion characteristics of tracked-wheel robots, this method models the odometry for each mode separately and non-holonomic constrained (NHC) velocity model [12]. By installing odometry sensors on both sides of the tracked-wheel robot, differential odometry measures the actual operating state of the robot's center, and calculates the differential odometry heading angle to compensate for the system's heading angle error, effectively suppressing heading divergence. This establishes the odometer measurement equipment for tracked-wheel robots, designs a self-localization system for these robots, and formulates the odometer measurement apparatus and INS error equations. The paper derives a combined localization algorithm for tracked-wheel robots. Experimental validation of the proposed method's feasibility was conducted through tracked-wheel robot localization experiments, demonstrating that the localization accuracy meets the requirements for autonomous tracked-wheel robot localization. By proposing a combined localization method based on inertial navigation and odometer (INS/OD), this study successfully addresses the localization challenges arising from the mode transitions in the wheeled-track robot in sheltered space. The approach offers insights into addressing the positioning issues associated with multi-modal wheeled-track robots.

II. PRINCIPLES OF TRACKED-WHEEL ROBOT AUTONOMOUS LOCALIZATION

The combined localization approach for tracked-wheel robots based on Inertial Navigation System/Odometry (INS/OD) employs INS as the primary source of localization, supplemented by odometry. The principle of this method is illustrated in FIGURE 2.

(a) Collapse due to natural disaster

(b) Complex subterranean environment

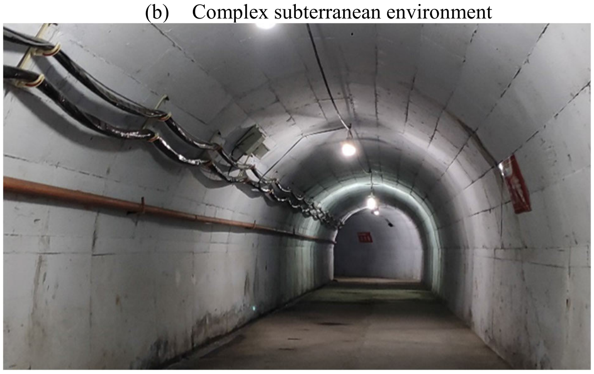

(c) Subterranean tunnel

FIGURE 1. Schematic diagram of a typical sheltered space.

The INS unit is positioned within the interior of the tracked-wheel robot, with odometer encoders located on both sides, coupled to the motor wheel axles of the robot. The process begins with the initial alignment of the tracked-wheel robot to obtain the initial attitude, which is then used to derive the initial attitude transformation matrix. During the robot's movement, information obtained from INS, including attitude, position, and velocity, is combined with odometry data, which calculates velocity and angular velocity of the heading angle. These values are utilized as observations and input into a closed-loop Extended Kalman Filter for data fusion. Subsequently, the position and attitude data output by the closed-loop Extended Kalman Filter are fed back to INS and OD data to reduce errors. This feedback mechanism helps minimize errors in the localization process.

A. WHEEL MODE OF TRACKED-WHEEL ROBOTS

1) WHEEL MODE MOTION SCENARIOS

A connecting plate is affixed to the robot's chassis, with a stepper motor mounted on the connecting plate. The front and rear sides of the wheel drive unit are equipped with guiding slide rail devices to facilitate vertical motion. The wheel drive unit's left and right sides are connected to two wheels for driving purposes. The robot's tracks are raised, with all four wheels in contact with the ground, as illustrated in FIGURE 3. This mode is designed to meet the robot's requirements for long-distance, high-speed, and efficient movement. It allows flexible forward and backward motion, as well as turning, reducing the robot's footprint and minimizing friction.

2) WHEEL MODE ODOMETRY MODELING

As depicted in FIGURE 4, the odometer device is fixed to the left and right wheels (or tracks) of the robot's chassis and is connected to the motors. It mainly consists of two orthogonal optical encoders, two active wheels, motors, and related transmission mechanisms.

In FIGURE 4, the active wheels rotate in the same direction as the robot's forward movement, driving the encoders to rotate. This rotation provides incremental pulse counts ΔN_{1L} and ΔN_{1R} for the left and right active wheels within a unit of time, respectively. By calculating these counts, the incremental mileage along the robot's longitudinal axis in the forward direction can be obtained for the left and right active wheels as ΔS_{1L} and ΔS_{1R}. ΔS_1 represents the forward mileage increment of the tracked-wheel robot in the wheel mode:

$$\Delta S_{1L} = \Delta N_{1L} \times \frac{L_1}{N_0} \times \mathrm{i}_1 \tag{1}$$

$$\Delta S_{2R} = \Delta N_{1R} \times \frac{L_1}{N_0} \times \mathrm{i}_1 \tag{2}$$

$$\Delta S_1 = \frac{\Delta S_{1L} + \Delta S_{1R}}{2} \tag{3}$$

L_1 represents the wheel circumference, the encoder precision is denoted as N_0, and i_1 stands for the transmission ratio between the motor and the twin active wheels in the wheeled mode.

B. TRACKED MODE OF TRACKED-WHEEL ROBOTS

1) TRACKED MODE MOTION SCENARIOS

As shown in FIGURE 5, slide rail devices are attached to the front and rear sides of the wheel drive unit to facilitate the upward and downward movement of the tracks. The left and right sides of the track drive unit are equipped with two wheels. This mode primarily employs dual-wheel drive as the fundamental mode of operation, with the tracks positioned below to assist in enhancing the robot's obstacle-crossing capabilities. With the tracks positioned below, the robot increases its contact area with the ground, enabling it to adapt to various terrain conditions, including soft, muddy, swampy, and uneven terrains.

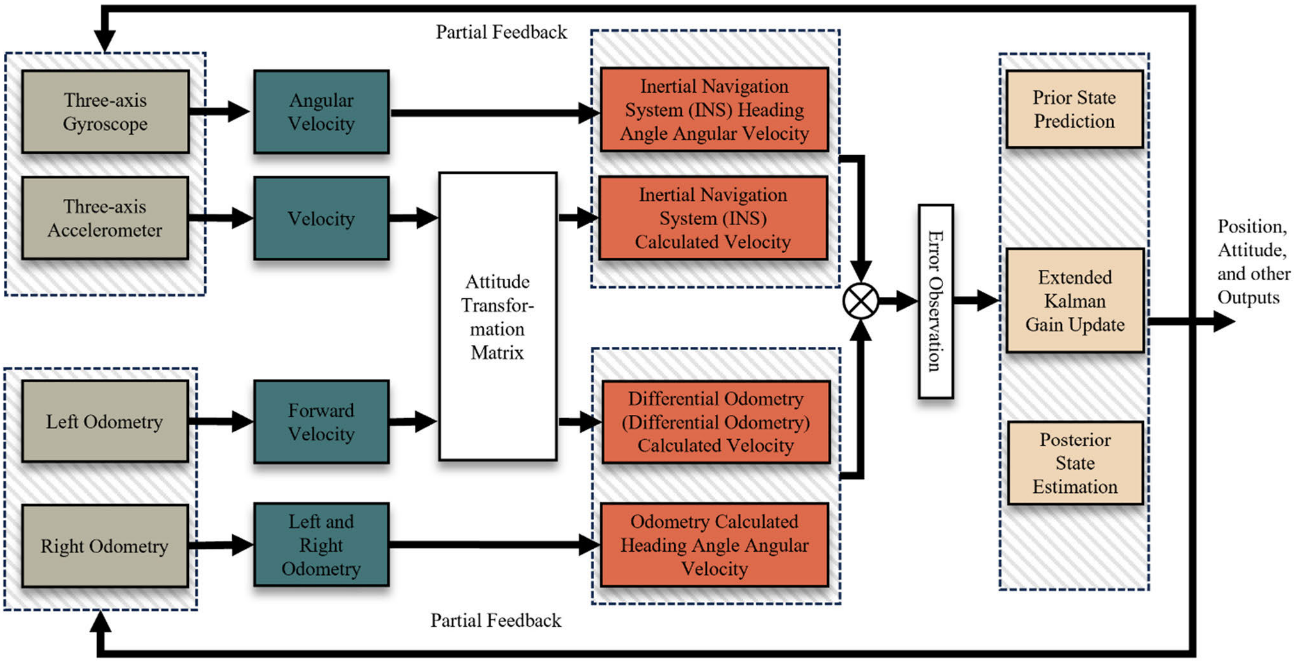

FIGURE 2. Principle of wheeled-track robot integrated positioning based on INS/OD.

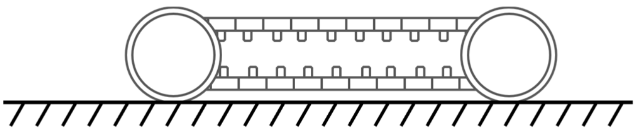

FIGURE 3. Schematic diagram of wheel mode motion.

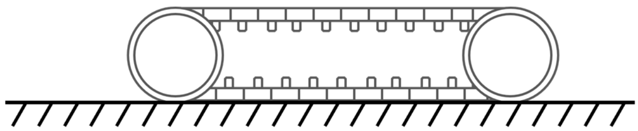

FIGURE 5. Schematic diagram of tracked mode motion.

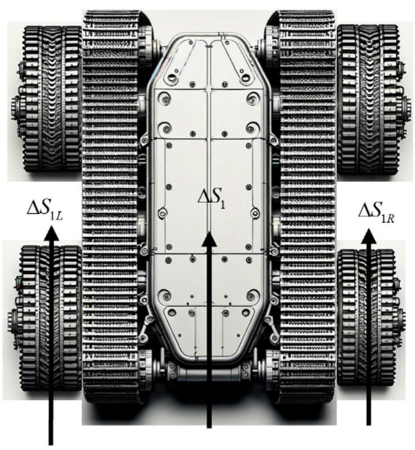

FIGURE 4. Simplified schematic diagram of wheel mode odometry motion modeling.

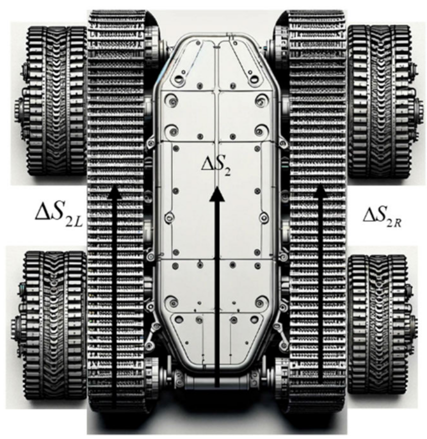

FIGURE 6. Schematic diagram of tracked mode odometry modeling.

2) TRACKED MODE ODOMETRY MODELING

As depicted in FIGURE 6, the odometer device in the tracked mode is fixed to the left and right wheels (or tracks) of the robot's chassis and is connected to the motors. It mainly consists of two orthogonal optical encoders, two active wheels coupled with the tracks, motors, and related transmission mechanisms.

The principle of track mileage measurement involves the use of 2 encoders, which are respectively mounted on the track and connected to the active wheel through a differential gear. As the track rotates with the forward motion of the tracked-wheel robot, it acquires the number of encoder pulses

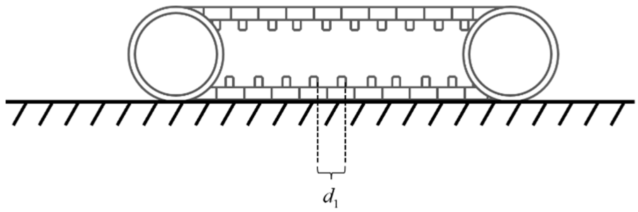

FIGURE 7. Illustrates the schematic diagram of the distance between the track gears.

read in unit time Δt, denoted as ΔN_{2L} and ΔN_{2R} for the left and right sides, respectively. Thus, the distances traveled by the left and right tracks, as well as the overall motion of the tracked-wheel robot, are given by:

$$\Delta S_{2L} = \Delta N_{2L} \times \frac{L_2}{N_0} \times \mathrm{i}_2 \tag{4}$$

$$\Delta S_{2R} = \Delta N_{2R} \times \frac{L_2}{N_0} \times \mathrm{i}_2 \tag{5}$$

$$\Delta S_2 = \frac{\Delta S_{2L} + \Delta S_{2R}}{2} \tag{6}$$

Here, i_2 represents the ratio between the odometer's active wheel motor and the track drive in track mode, and L_2 corresponds to the distance covered when the wheel, fixed to the track gear, rotates one revolution.

$$L_2 = n \times d_1 \tag{7}$$

In (7), as shown in FIGURE 7, d_1 represents the distance between the two gears of the track, and n stands for the number of teeth engaged by the track gear when it completes one revolution.

C. ODOMETER HEADING ANGLE COMPUTATION

As shown in (8), when the wheeled-track robot is in the wheeled mode, the odometer measures the mileage increment ΔS within the time unit Δt as follows:

$$\Delta S = \Delta S_1 \tag{8}$$

As shown in (9), when the wheeled-track robot is in the wheeled mode, the odometer measures the mileage increment ΔS within the time unit Δt as follows:

$$\Delta S = \Delta S_2 \tag{9}$$

In summary, the velocity v_D of the wheeled-track robot within the time unit Δt is given by (10):

$$v_D = \frac{\Delta S}{\Delta t} \tag{10}$$

Next, model the motion for the odometer heading angle.

As shown in FIGURE 8, let ΔS_L be the distance increment measured by the left odometer, and ΔS_R be the distance increment measured by the right odometer within the time unit T.

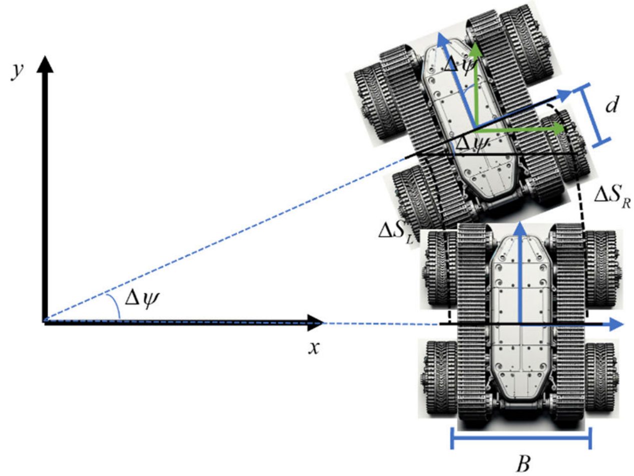

FIGURE 8. Illustrates the computation of the heading angle constraints.

When the wheeled-track robot is in the wheeled mode, the left odometer and right odometer measure the distance increments ΔS_L and ΔS_R within the time unit Δt as follows:

$$\Delta S_L = \Delta S_{1L} \tag{11}$$

$$\Delta S_R = \Delta S_{1R} \tag{12}$$

In the case of the track mode of the wheeled-track robot, the left odometer and right odometer measure the distance increments ΔS_L and ΔS_L within the time unit Δt as follows:

$$\Delta S_L = \Delta S_{2L} \tag{13}$$

$$\Delta S_R = \Delta S_{2R} \tag{14}$$

As depicted in FIGURE 8, the displacement change of the left and right dual odometers, denoted as d, is given by (15):

$$d = \Delta S_L - \Delta S_R \tag{15}$$

The distance between the two drive wheels of the robot is B. Therefore, the change in heading angle $\Delta\psi$ of the wheeled-track robot within the time unit Δt is calculated as:

$$\Delta\psi \approx \sin(\Delta\psi) = \frac{d}{B} \tag{16}$$

The angular velocity w has a magnitude of:

$$w = \frac{\Delta\psi}{\Delta t} \tag{17}$$

D. RECOGNITION OF ODOMETER CALIBRATION FOR DIFFERENT MODES

During the operation, the wheeled-track robot undergoes structural transformations based on the distinct characteristics of different ground environments. In the process of implementing the localization algorithm, it is essential to first process and identify the odometer data for the two different motion modes.

When the wheeled-track robot switches between motion modes, it must first come to a halt and then proceed with the motion mode change. However, during normal straight-line travel of the wheeled-track robot, the velocity v_D calculated by the odometer matches the forward velocity V_y calculated by the INS. This equivalence allows the distinction between different motion modes through the differing odometer calibrations.

Within a unit of time, the ratio of the forward displacement ΔS_{INS} calculated by the INS to the increment in the odometer pulse count ΔN is compared with the odometer calibrations K_D for both motion modes to determine the robot's current motion mode. As shown in (18), K_{D1} represents the odometer calibration for the wheeled mode. When the difference between these values satisfies the following relationship, the wheeled-track robot is in the wheeled mode, and the calibration K_{D1} is used to calculate the distance obtained from the odometer:

$$\left\| \frac{\Delta S_{INS}}{\Delta N} - K_{D1} \right\| < \Lambda_1 \tag{18}$$

Similarly, the ratio of the forward displacement ΔS_{INS} to the increment in the odometer pulse count ΔN is compared with the odometer calibration K_{D2} for the track mode, and when the difference satisfies the following relationship, the wheeled-track robot is in the track mode, and the calibration K_{D2} is used to calculate the distance obtained from the odometer:

$$\left\| \frac{\Delta S_{INS}}{\Delta N} - K_{D2} \right\| < \Lambda_2 \tag{19}$$

In (18) and (19), A1 and A2 represent threshold values that have been set. The selection of Λ_1 and Λ_2 depends on factors such as the vehicle's traveling speed, INS velocity errors, and odometer measurement noise.

III. COMBINED LOCALIZATION SYSTEM MODEL

The coordinate systems for localization are illustrated in FIGURE 9, with the East-North-Up ($O-X_nY_nZ_n$) coordinate system chosen as the navigation coordinate system (n-frame) and the right-front-up ($O' - X_bY_bZ_b$) chosen as the body coordinate system (b-frame).

In the challenging environment of sheltered spaces where wheeled-track robots operate, various motion mode switches lead to the collection of diverse odometry data. Due to the complexity of the environment and the significant differences in data, obtaining accurate statistical characteristics of noise becomes challenging. To address this, the proposed approach employs Extended Kalman Filtering for the design of a combined localization-oriented filter. System errors are chosen as the states of the combined localization filter, primarily composed of errors from the dead reckoning equations [13]. Initially, a continuous model of the combined navigation system is established based on the error equations. Subsequently, discretization is performed, and through discrete closed-loop feedback Extended Kalman Filtering, errors in the inertial navigation system are estimated and compensated for.

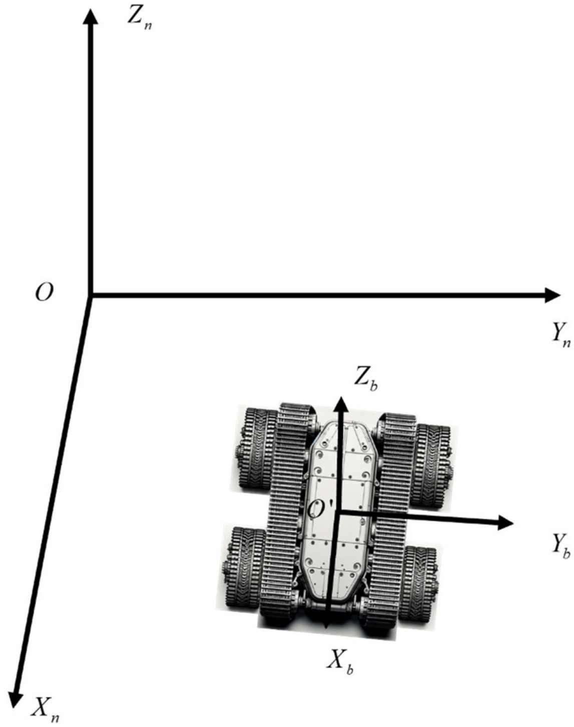

FIGURE 9. Localization coordinate systems.

A. INERTIAL NAVIGATION SYSTEM ERROR EQUATIONS

The attitude angle error equation is given by:

$$\delta\dot{\phi} = -\left(\omega_{ie}^n + \omega_{en}^n\right)\boldsymbol{\varphi} - \left(\delta\omega_{ie}^n + \delta\omega_{en}^n\right) - \boldsymbol{C}_b^n\varepsilon^b \tag{20}$$

The velocity error equation is expressed as:

$$\begin{aligned}\delta\dot{\boldsymbol{v}}^n &= f^n\boldsymbol{\varphi} - \left(2\omega_{ie}^n + \omega_{en}^n\right)\delta\boldsymbol{v}^n - \\ &\left(2\delta\omega_{ie}^n + \delta\omega_{en}^n\right)\boldsymbol{v}^n + \boldsymbol{C}_b^n\nabla^b\end{aligned} \tag{21}$$

The position error equation is defined as:

$$\begin{cases} \delta\dot{L} = \dfrac{\delta v_{\mathrm{E}}^n}{R_{\mathrm{M}}+h} - \dfrac{v_{\mathrm{N}}^n\delta h}{(R_{\mathrm{M}}+h)^2} \\ \delta\dot{\lambda} = \dfrac{\left(\delta v_{\mathrm{N}}^n \sec L + v_{\mathrm{E}}^n \sec L \tan L\right)}{(R_{\mathrm{N}}+h)} - \dfrac{v_{\mathrm{E}}^n \sec L\delta h}{(R_{\mathrm{N}}+h)^2} \\ \delta\dot{h} = \delta v_{\mathrm{U}}^n \end{cases} \tag{22}$$

In (20), (21), and (22), $\boldsymbol{\varphi} = \left[\phi_{\mathrm{E}}\phi_{\mathrm{N}}\phi_{\mathrm{U}}\right]^{\mathrm{T}}$ represents the platform error angle computed by strapdown inertial navigation. ε^b stands for gyroscope drift, $\delta\boldsymbol{v}^n = \left[\delta v_{\mathrm{E}}\delta v_{\mathrm{N}}\delta v_{\mathrm{U}}\right]$ denotes velocity error, ∇^b indicates the accelerometer bias in the robot's coordinate system, and δL, $\delta\lambda$, and δh correspond to errors in latitude, longitude, and altitude, respectively. A comprehensive derivation of the above equations can be found in the referenced literature [14].

B. SYSTEM STATE EQUATIONS AND OBSERVATION EQUATIONS

Combining the errors from INS calculations and navigation computation, a 15-dimensional state vector is formed as follows:

$$X = \left[(\delta p_{INS})^T (\delta \boldsymbol{v}^n)^T \ (\delta \phi)^T \ (\boldsymbol{\varepsilon}^b)^T (\nabla^b)^T\right] \tag{23}$$

In (23): $\delta p_{INS} = \left[\, \delta L \ \delta\lambda \ \delta h \,\right]^T$ represents the 3D position error computed by the inertial navigation system (INS); $\delta \boldsymbol{v}^n$ is the 3D velocity error; $\delta\phi$ denotes the 3D attitude error; $\boldsymbol{\varepsilon}^b$ is the gyroscope bias error; and ∇^b stands for the accelerometer bias error.

NHC velocity model is established, and this study adopts the constraint of the vehicle's lateral velocity being zero [15], [16]. The difference between the INS forward-calculated velocity and the odometry (OD) forward-calculated velocity is used as the second observation [17], [18], [19], while the difference between the gyroscope's yaw rate and the differential odometry-calculated yaw rate is employed as the third observation. The system measurement equation is formulated as follows:

$$\boldsymbol{Z} = \begin{bmatrix} V_x - 0 \\ \boldsymbol{V}_y - \boldsymbol{V}_{\mathrm{D}}^n(2) \\ w_{ib}(2) + \varepsilon_Z^b - w \end{bmatrix} \tag{24}$$

In (24), $\boldsymbol{V}_y$ represents the INS-calculated forward velocity projected in the navigation coordinate system, $\boldsymbol{V}_{\mathrm{D}}^n(2)$ is the forward velocity projected in the navigation coordinates by odometry, $w_{ib}(2)$ is the INS-measured yaw rate, ε_Z^b is the gyroscope's Z-axis bias, and w is the differential odometry-calculated angular rate.

Hence, the INS/OD combined localization state-space model is established as follows:

$$\begin{cases} \boldsymbol{X}_k = \boldsymbol{\Phi}_{k/k-1}\boldsymbol{X}_{k-1} + w_{k-1} \\ \boldsymbol{Z}_k = \boldsymbol{H}_k\boldsymbol{X}_k + V_k \end{cases} \tag{25}$$

$$H = \begin{bmatrix} 0 & C_{\mathrm{n}}^{\mathrm{b}}(1, 1:3) & 0 & 0 & 0 \\ 0 & C_{\mathrm{n}}^{\mathrm{b}}(2, 1:3) & 0 & 0 & 0 \\ 0 & 0 & 0 & [0\ 0\ 1] & 0 \end{bmatrix} \tag{26}$$

In (25) and (26): $\boldsymbol{X}_k$ is the state vector at time k; $\boldsymbol{\Phi}_{k/k-1}$ is the state transition matrix; w_{k-1} is the system process noise at time $k-1$; $\boldsymbol{Z}_k$ is the observed value at time k. V_k is the measurement white noise at time k. $\boldsymbol{H}_k$ is the measurement matrix at time k; $C_{\mathrm{n}}^{\mathrm{b}}$ is the attitude transformation matrix.

C. COMBINED LOCALIZATION ALGORITHM BASED ON CLOSED-LOOP EXTENDED KALMAN FILTER FEEDBACK

As illustrated in FIGURE 10, the combined navigation system matches the positional change information obtained from odometry (OD) and inertial navigation system (INS) calculations. It utilizes closed-loop state feedback to adjust parameters such as position, velocity, attitude, inertial device biases, and odometry error parameters. Simultaneously, it combines INS-calculated position and attitude information to output the optimal solution.

The state equation is discretized, and the filtering is performed through the following steps:

i Compute the a priori estimate of the state:

$$\hat{\boldsymbol{X}}_k^- = \boldsymbol{\Phi}_{k/k-1}\hat{\boldsymbol{X}}_{k-1} \tag{27}$$

In (27), $\hat{\boldsymbol{X}}_{k-1}$ is the a posteriori estimates of the state at times $k-1$, respectively.

ii Calculate the a priori estimate of the mean square error:

$$\boldsymbol{P}_{k/k-1} = \boldsymbol{\Phi}_{k/k-1}\boldsymbol{P}_{k-1}\boldsymbol{\Phi}_{k/k-1}^{\mathrm{T}} + \boldsymbol{Q}_{k-1} \tag{28}$$

In (28), $\boldsymbol{Q}_{k-1}$ is the process noise covariance matrix at time $k-1$, and $\boldsymbol{P}_{k/k-1}$ is the estimated error covariance matrix for one-step prediction.

iii Update the Extended Kalman Filter (EKF) gain $\boldsymbol{K}_k$:

$$\boldsymbol{K}_k = \boldsymbol{P}_{k/k-1}\boldsymbol{H}_k^{\mathrm{T}}(\boldsymbol{H}_k\boldsymbol{P}_{k/k-1}\boldsymbol{H}_k^{\mathrm{T}} + \boldsymbol{R}_k)^{-1} \tag{29}$$

In (29), $\boldsymbol{R}_k$ is the measurement noise covariance matrix at time k.

iv The algorithm employs closed-loop feedback correction [20], [21] to reduce errors, adjusting the error amount after each filtering and then outputting. By setting $\boldsymbol{X''}$ to 0 in $\hat{\boldsymbol{X}}_k = \hat{\boldsymbol{X}}_{k-1} + K_k\left(\boldsymbol{Z}_k - H\hat{\boldsymbol{X}}_{k-1}\right)$ of the traditional Extended Kalman Filter, the simplified posterior state estimate is as follows:

$$\hat{\boldsymbol{X}}_k = \boldsymbol{K}_k\boldsymbol{Z}_k \tag{30}$$

v Update the mean square error:

$$\boldsymbol{P}_k = (I - \boldsymbol{K}_k\boldsymbol{H}_k)\boldsymbol{P}_{k/k-1}(I - \boldsymbol{K}_k\boldsymbol{H}_k)^T + \boldsymbol{K}_k\boldsymbol{R}_k\,(\boldsymbol{K}_k)^T \tag{31}$$

Using the a posteriori estimate of the error, $\hat{\boldsymbol{X}}_k$ becomes the optimal estimate of the state. The error-corrected INS-calculated position yields the desired position.

IV. EXPERIMENTAL VALIDATION AND DATA ANALYSIS

A. EXPERIMENTAL PLATFORM SETUP

The experimental platform for combined localization of tracked-wheel robots based on Inertial Navigation System/Odometry (INS/OD) includes the tracked-wheel robot, DETA100R4G-INS, DETA100R4G series RTK modules, and four odometry sensors mounted on both sides of the tracked-wheel robot. To ensure real-time and continuous localization, the INS and OD outputs in this experiment are sampled at a high frequency of 100Hz. The experimental site is divided into indoor and outdoor areas, both characterized by complex terrains, with the overall dimensions of the tracked-wheel robot being 0.319m in height, 0.766m in length, an active wheelbase of 0.671m, and a track spacing of 0.650m. The position of the tracked-wheel robot obtained from the DETA100R4G series RTK modules serves as the reference for the experiment, validating the accuracy of the INS/OD combined localization. The INS parameters are detailed in TABLE 1. The navigation host collects raw navigation data, and using quaternion pose calculation methods and the fusion algorithm proposed in this paper, calculates the position coordinates of the tracked-wheel robot. The results are then transmitted to a remote monitoring device via a communication module.

Equipment installation is illustrated in FIGURE 11. The center of gravity coordinates of the tracked-wheel

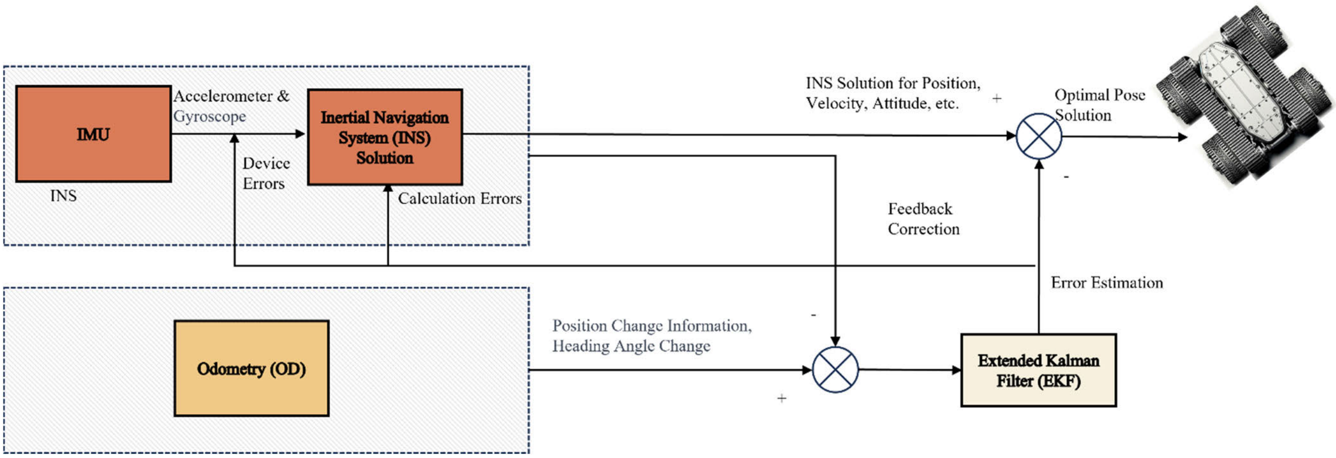

FIGURE 10. Schematic diagram of closed-loop extended Kalman filter feedback algorithm.

TABLE 1. Parameters of DETA100R4G inertial measurement unit.

Symbol	Accelerometer	Gyroscope
Range	±16(g)	±400(° /s)
Scale Factor Error	300(ppm)	1000(ppm)
Bias Instability	40(ug)	Less than 10°/hr, the redundant heading gyro is maintained at 2°/hr.
Linearity	<0.1(%FS)	<0.1(%FS)
Noise Density	75(ug/√Hz)	0.0028(° /s/ √ Hz)
Bandwidth	500(Hz)	500(Hz)
Orthogonality Error	±0.05(°)	±0.05(°)

TABLE 2. Odometer parameters.

Parameters	Wheeled Mode Odometer	Tracked Mode Odometer
Resolution($P \cdot R^{-1}$)	500	500
Scale Factor($m \cdot P^{-1}$)	2.26888×10^{-5}	1.5295×10^{-5}

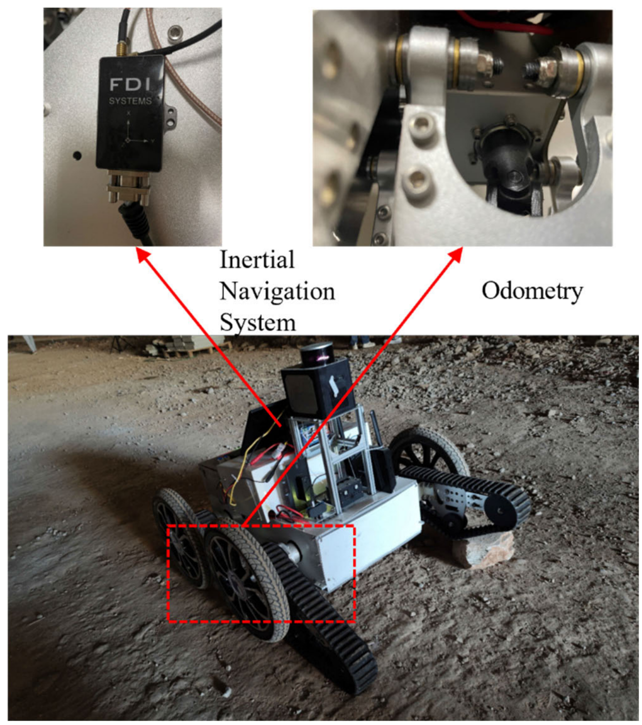

FIGURE 11. Schematic of wheeled-track robot localization experimental system.

robot are considered as the overall position reference. The DETA100R4G-INS is mounted on the upper side of the tracked-wheel robot near the center to minimize velocity errors induced by the robot's rotation. Each of the left and right rear active wheels is connected to an odometer via a gear mechanism. Similarly, each of the left and right tracks is connected to an odometer through a gear mechanism. The odometer error parameters are detailed in TABLE 2.

B. EXPERIMENTAL PROCEDURE AND RESULT ANALYSIS

1) OUTDOOR LOCALIZATION EXPERIMENT

The wheeled-track robot conducted experiments multiple times under the same outdoor test conditions, and a specific set of experimental data was selected for analysis. The initial alignment of the wheeled-track robot was performed based on the starting latitude and longitude information provided by the RTK module. After alignment, the Inertial Navigation System (INS) calculated the initial attitude transformation matrix. The experiment simulated the operational modes required for the wheeled-track robot in practical scenarios, encompassing wheeled mode, tracked mode, the transition process between wheeled and tracked modes, as well as the transition from tracked to wheeled mode.

As illustrated in FIGURE 12, the movement of the wheeled-track robot unfolded as follows: initially traveling in wheeled mode on a flat section (Segment A) for 34.7 seconds, then pausing for 7.76 seconds at Segment B, during

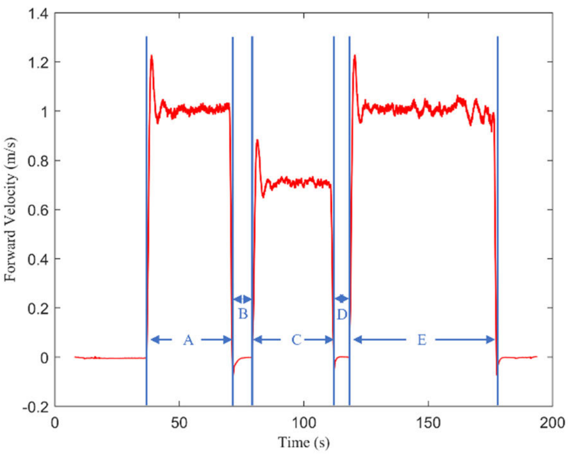

FIGURE 12. Schematic of wheeled-tracked robot's forward Velocity.

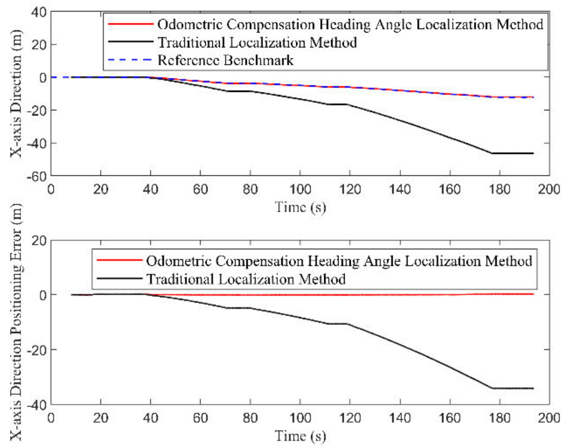

FIGURE 13. Analysis of wheeled-track robot's X-axis displacement.

TABLE 3. Initial position and posture data of tracked-wheel robots.

Parameters	Gyroscope
Heading Angle (°)	6.82
Roll Angle (°)	0.6986
Pitch Angle (°)	-0.5191
Longitude (°)	116.3403
Latitude (m)	40.0357
Altitude (m)	45.293
Local Gravitational Acceleration(m/s^2)	9.8812

TABLE 4. X-axis and Y-axis positioning errors of the proposed method.

	Maximum Localization Error	Average Localization Error	Localization Error Variance
X-Axis Direction	0.2228m	0.015 m	0.0116
Y-Axis Direction	0.3258m	0.0744m	0.0180

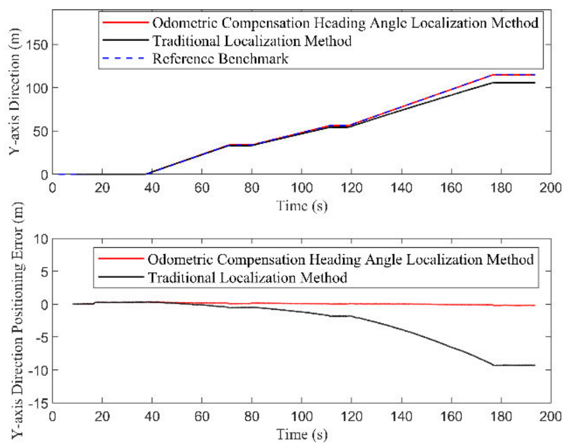

FIGURE 14. Analysis of wheeled-track robot's Y-axis displacement.

which the robot transitioned from wheeled to tracked mode. Subsequently, in tracked mode, it traversed a complex terrain with undulations, soft ground, and mud at Segment C, taking 32.94 seconds. After a 6.1-second pause at Segment D, the robot switched back from tracked to wheeled mode. Finally, the wheeled-track robot traveled through a flat section (Segment E) in wheeled mode for 59.34 seconds. The entire experimental process lasted for a total duration of 193.76 seconds, covering a cumulative displacement of 117.04 meters.

Simultaneously updating the attitude transformation matrix and velocity, the robot's left and right odometers recorded the distances traveled by each side. Computational procedures yielded the robot's velocity and heading angle. The Extended Kalman Filter (EKF) fused data from both sources, correcting the heading angle of the odometer model and compensating for INS calculation errors. The initial pose data for the wheeled-track robot is presented in TABLE 3.

The RTK trajectory was employed as the positioning reference benchmark, and a comparative analysis was conducted with the trajectories obtained using the method proposed in this paper. The wheeled-track robot's latitude and longitude coordinates were converted to Cartesian coordinates in the Gauss coordinate system and compared with the initial coordinates [22]. This process yielded the displacement along the X-axis and Y-axis of the wheeled-track robot. FIGURE 13 and FIGURE 14 demonstrate that the positioning errors in the X and Y directions, measured using the proposed positioning method, did not diverge over time. In comparison with the traditional Extended Kalman Filter (EKF) [12], positioning method, the proposed method exhibited excellent tracking performance concerning the actual trajectory.

As depicted in FIGURE 15, FIGURE 16, and FIGURE 17, it is evident that, with the passage of time, the positioning errors in the wheeled-track robot obtained by the traditional EKF positioning method gradually increased. In contrast, the displacements derived from the proposed combination positioning method closely aligned with the actual displacements obtained from the RTK benchmark. The heading angle error in the proposed combination positioning method was smaller than that in the traditional EKF positioning method. As depicted in TABLE 5, the average positioning error in

TABLE 5. Error comparison of localization methods.

	Maximum Localization Error (Percentage of Total Distance Traveled)	Average Localization Error	Localization Error Variance
The Proposed Method in This Paper	0.2228m	0.015 m	0.0116
Traditional EKF Localization Method	0.3258m	0.0744m	0.0180

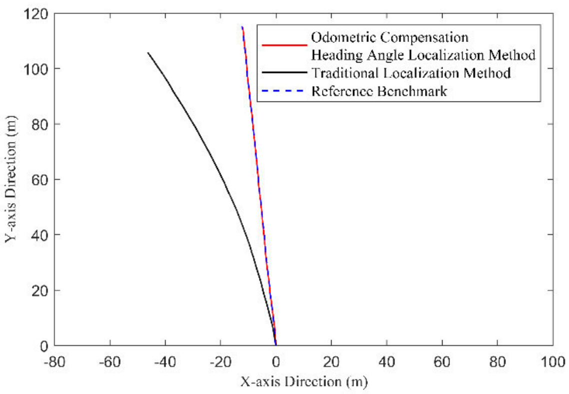

FIGURE 15. Schematic of wheeled-track robot's trajectory.

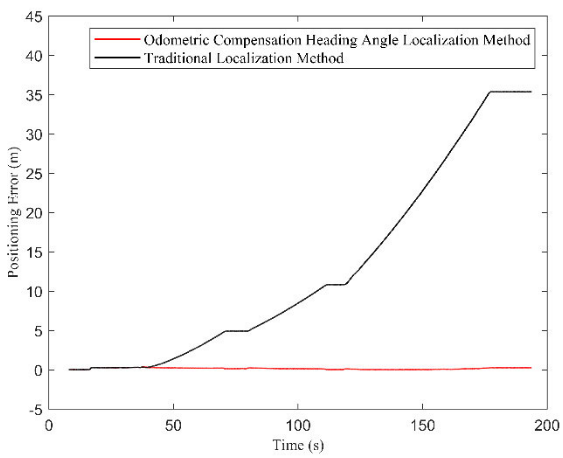

FIGURE 16. Wheeled-track robot's positioning error.

the combination positioning method was 98.72% lower than that calculated by the traditional EKF positioning method. Specifically, the maximum positioning error obtained by the combination positioning method was 0.3578 meters, the average positioning error was 0.1611 meters, and the variance was 0.0093. The maximum error was merely 0.31% of the total traveled distance. Consequently, it can be concluded that the proposed method meets the positioning accuracy requirements for wheeled-track robots.

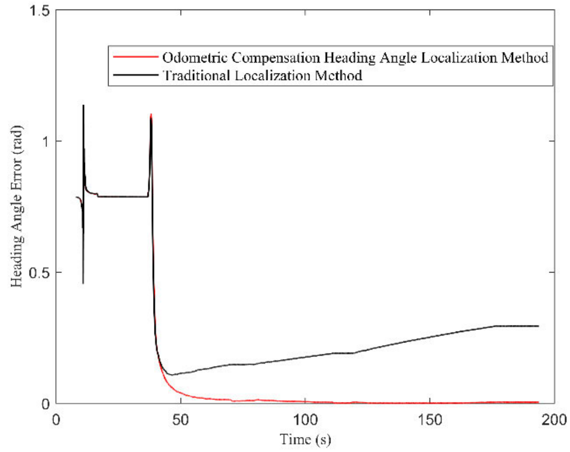

FIGURE 17. Wheeled-track robot's heading angle error.

FIGURE 18. Experiment environment in underground tunnel.

2) UNDERGROUND LOCALIZATION EXPERIMENTS

As shown in FIGURE 18, multiple sets of experiments were conducted with The wheeled-track robot in a typical obstructed environment, namely an underground tunnel, and a specific set of experimental data was chosen for analysis. The experimental method for The wheeled-track robot's localization involved relative positioning. After starting from the initial point, The wheeled-track robot returned to the starting point, and accuracy was calculated based on the distance between the starting and ending points. The operational modes required for The wheeled-track robot's actual work, including wheel mode, track mode, the transition process between wheel and track modes, and the transition process between track and wheel modes, were controlled.

As illustrated in FIGURE 19, direction representation by velocity sign, the movement process of The Wheeled-Track Robot is described as follows: Initially, it travels in wheeled mode through the flat segment A, taking 14.4 seconds. Subsequently, during the pause of 10 seconds in segment B, the robot transitions from wheeled mode to tracked mode. It then

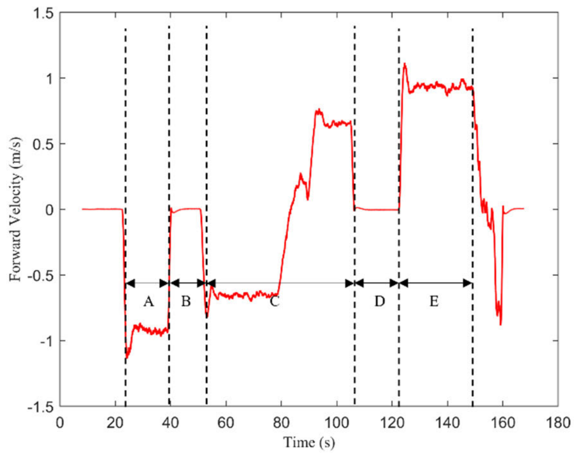

FIGURE 19. Velocity along the Y-axis.

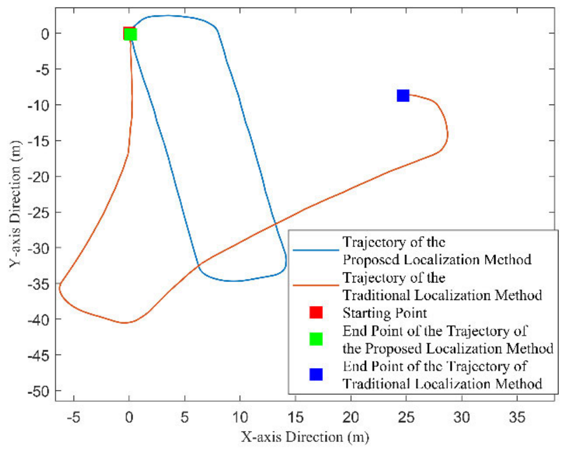

FIGURE 20. Trajectory map of underground tunnel localization experiment.

travels through the uneven and challenging segment C, characterized by soft and muddy terrain, taking 49.24 seconds. Another pause of 16.22 seconds in segment D involves the transition from tracked mode to wheeled mode. Finally, the wheeled-track robot traverses the flat segment E in wheeled mode, taking 25.22 seconds. The entire experimental process lasts for a total duration of 167.56 seconds, with the robot covering a cumulative displacement of 92.94 meters.

As depicted in FIGURE 20, with the passage of time, the displacement error of The Wheeled-Track Robot obtained by the traditional EKF localization method gradually increases. Meanwhile, the combination localization method proposed in this paper exhibits higher precision, as indicated in TABLE 6. The positioning error of the proposed combination localization method is 0.2143m, accounting for 0.2306% of the total distance. In contrast, the positioning error of the traditional EKF localization method is 26.2229m, constituting 28.2129% of the total distance. It can be concluded that the proposed method in this paper achieves satisfactory underground experimental positioning accuracy for The Wheeled-Track Robot.

TABLE 6. Error comparison of localization methods.

	Localization Error (Percentage of Total Distance) between Trajectory End and Start Points
The Proposed Method in This Paper	0.2143m(0.2306%)
Traditional EKF Localization Method	26.2229m(28.2129%)

V. CONCLUSION

In response to the localization challenges caused by the multi-mode switching of wheeled-track robots, a combined localization method based on Inertial Navigation System/Odometry (INS/OD) is proposed. This method leverages the advantages of being unaffected by external signals, having a high data update rate, and providing comprehensive data. It significantly reduces cumulative errors, thereby enhancing the tracking accuracy of the wheeled-track robot's trajectory.

In sheltered space, the wheeled-track robot underwent practical localization tests in both outdoor and underground tunnel environments. The results demonstrate that the proposed combined localization method achieves a positioning error within 0.3578m for outdoor absolute localization, accounting for only 0.31% of the total distance traveled in the outdoor experiment. The average error is 0.1611m. For underground tunnel relative localization, the positioning error is 0.2143m, representing only 0.2306% of the total tunnel distance. Both experiments validate the effectiveness of the proposed approach in mitigating the impact of inertial navigation cumulative errors on wheeled-track robot localization. The feasibility and superiority of the proposed method are confirmed, establishing a foundation for wheeled-track robot navigation and providing a reliable and stable positioning solution for multi-modal robots.

The current study is confined to planar localization. Future research should delve deeper into aspects such as environmental adaptability, algorithm robustness, and the application of machine learning to advance the development of three-dimensional localization in this field. Exploring how to better integrate information from other sensors, enhancing the system's perception, and adaptability to complex environments, as well as refining strategies for multi-modal mode transitions, will be crucial for further advancements.

REFERENCES

[1] R. U. I. Hong-Bin, L.-L. Li, W. Cao, T.-C. Wang, K.-W. Duan, and Y.-H. Wu, "Gait planning and obstacle-surmounting performance analysis of wheel-track-leg composite bionic robot," *Chin. J. Eng. Design*, vol. 29, no. 2, pp. 133–142, 2022.

[2] F. Cao, Y. Zhuang, F. Yan, Q. F. Yang, and W. Wang, "Long-term autonomous environment adaptation of mobile robots: State-of-the-art methods and prospects," *Acta Autom. Sinica*, vol. 46, no. 2, pp. 205–221, 2020.

[3] Y. Hu, X. Li, X. Dong, D. Kong, Q. Xu, and Y. Sun, "A reliable cooperative fusion positioning methodology for intelligent vehicle in non-line-of-sight environments," *IEEE Trans. Instrum. Meas.*, vol. 71, pp. 1–11, 2022.

[4] Y. Gao, J. Yuan, J. Jiang, Q. Sun, and X. Zhang, "VIDO: A robust and consistent monocular visual-inertial-depth odometry," *IEEE Trans. Intell. Transp. Syst.*, vol. 24, no. 3, pp. 2976–2992, Mar. 2023.

[5] W.-D. Ding, D. Xu, X.-L. Liu, D.-P. Zhang, and T. Chen, "Review on visual odometry for mobile robots," *Zidonghua Xuebao/Acta Autom. Sinica*, vol. 44, no. 3, pp. 385–400, 2018.

[6] J. Zheng, S. Li, S. Liu, Q. Fu, Y. Tao, and J. Li, "Positioning method of a shearer based on inertial navigation and LiDAR," *Zhongguo Guanxing Jishu Xuebao/J. Chin. Inertial Technol.*, vol. 28, no. 5, pp. 595–602, 2020.

[7] J. Gao, K. Li, and J. Chen, "Research on the integrated navigation technology of SINS with couple odometers for land vehicles," *Sensors*, vol. 20, no. 2, p. 546, Jan. 2020.

[8] S. Li, F. Huang, S. Qiu, and C. Fan, "SINS/Odometer integrated navigation method based on adaptive strong tracking filter," *Zhongguo Guanxing Jishu Xuebao/J. Chin. Inertial Technol.*, vol. 26, no. 2, pp. 156–161, 2018.

[9] Y. Shen, P. Wang, X. Ji, W. Zheng, and M. Wu, "Research on autonomous navigation method of roadheader aided by two-dimensional mileage," *Chin. J. Sci. Instrum.*, vol. 42, no. 11, pp. 96–105, 2021.

[10] H.-S. Zhao, L.-J. Miao, and H.-J. Shao, "Application of two-stage H_∞ filter in SINS/odometer integrated navigation system," *Zhongguo Guanxing Jishu Xuebao/J. Chin. Inertial Technol.*, vol. 23, no. 5, pp. 615–623, 2015.

[11] M. A. Hongwei, Z. Pu, M. A. O. Qinghua, and Z. Ying, "Research on positioning method of underground robot based on strapdown inertial navigation and odometer," *Gong-Kuang Zidonghua*, vol. 45, no. 4, pp. 35–42, 2019.

[12] P. Yu, W. Wei, J. Li, F. Wang, L. Zhang, and Z. Chen, "An improved autonomous inertial-based integrated navigation scheme based on vehicle motion recognition," *IEEE Access*, vol. 11, pp. 104806–104816, 2023.

[13] W. Ouyang, Y. Wu, and H. Chen, "INS/Odometer land navigation by accurate measurement modeling and multiple-model adaptive estimation," *IEEE Trans. Aerosp. Electron. Syst.*, vol. 57, no. 1, pp. 245–262, Feb. 2021.

[14] G. Yan and Y. Qin, "The study of vehicular RLG GPS/DR integrated navigation system," *J. Projectiles, Rockets, Missiles Guid.*, vol. 4, pp. 22–25, Sep. 2005.

[15] Q. Fu, Y. Liu, Z. Liu, S. Li, and B. Guan, "High-accuracy SINS/LDV integration for long-distance land navigation," *IEEE/ASME Trans. Mechatronics*, vol. 23, no. 6, pp. 2952–2962, Dec. 2018.

[16] Q.-W. Fu, Y.-Y. Qin, S.-H. Li, and H.-M. Wang, "Inertial navigation algorithm aided by motion constraints of vehicle," *Zhongguo Guanxing Jishu Xuebao/J. Chin. Inertial Technol.*, vol. 20, no. 6, pp. 640–643, 2012.

[17] X. Xu, J. Lai, P. Lv, J. Lu, S. Bai, and H. Hu, "High-precision positioning method of coal shearer in the underground environment based on rail kinematics model," *IEEE Access*, vol. 9, pp. 151198–151208, 2021.

[18] S. Wang and S. Wang, "Improving the shearer positioning accuracy using the shearer motion constraints in longwall panels," *IEEE Access*, vol. 8, pp. 52466–52474, 2020.

[19] Q. Chen, Q. Zhang, X. Niu, and Y. Wang, "Positioning accuracy of a pipeline surveying system based on MEMS IMU and odometer: Case study," *IEEE Access*, vol. 7, pp. 104453–104461, 2019.

[20] R. Si-Cong, "A cascade SINS/GNSS integrated navigation system with closed loop feedback," *J. Chin. Inertial Technol.*, 2003.

[21] C. Ti-Jing, "Simulation of rate azimuth inertial platform/log/gravity matching integrated navigation system," *J. Chin. Inertial Technol.*, 2005.

[22] Y. Gan, L. Sui, G. Qi, and H. Zhang, "A real-time attitude determination approach for land navigation based on GPS/gyroscope integration," *Wuhan Daxue Xuebao, Xinxi Kexue Ban/Geomatics Inf. Sci. Wuhan Univ.*, vol. 40, no. 3, pp. 379–383, 2015.

JIAZHEN LIN received the bachelor's degree in automation from Beijing Information Science and Technology University, Beijing, China, in 2021, where he is currently pursuing the master's degree in navigation guidance and control. His current research interests include integrated navigation, inertial navigation, and localization.

ZHONG SU (Member, IEEE) received the B.S. and M.S. degrees from Beijing Institute of Technology, in 1983 and 1989, respectively, and the Ph.D. degree from Beijing Institute of Vacuum Electronics Technology, in 1998. He is currently a Professor, the Ph.D. Supervisor, and the Director of Beijing Key Laboratory of High Dynamic Navigation Technology and the Director of the Key Laboratory of Modern Measurement and Control Technology, Ministry of Education of China, School of Automation, Beijing Information Science and Technology University, Beijing.

HUI ZHAO received the B.S. degree in intelligent science and technology and the M.S. degree in navigation guidance and control from Beijing Information Science and Technology University, Beijing, China, in 2014 and 2017, respectively, and the Ph.D. degree in navigation guidance and control from Beijing Institute of Technology, Beijing, in 2021. He is currently an Associate Researcher with Beijing Information Science and Technology University. His research interests include integrated navigation, inertial navigation, and visual navigation.

YUXIN ZHAO received the bachelor's degree in automation from Beijing Information Science and Technology University, Beijing, China, in 2021, where he is currently pursuing the master's degree in navigation guidance and control. His current research interest includes target detection.

XINKAI WANG was born in Liaoning, in 1997. He is currently pursuing the master's degree with Beijing Information Science and Technology University. His current research interest includes navigation and localization.

HAO ZHOU was born in Liaoning, in 1995. He is currently pursuing the master's degree with Beijing Information Science and Technology University. His current research interest includes robot motion control.